Nanocrystalline Ferroelectric $BiFeO_3$ Thin Films by Low Temperature Atomic Layer Deposition

Mariona Coll[1*], Jaume Gazquez[1], Ignasi Fina[2,3], Zakariya Khayat[4], Andy Quindeau[2], Marin Alexe[3], Maria Varela[5], Susan Trolier-McKinstry[4], Xavier Obradors[1], Teresa Puig[1]

[1]Institut de Ciencia de Materials de Barcelona (ICMAB-CSIC), Campus UAB, 08193, Bellaterra, Catalonia, Spain

[2]Max Planck Institute of Microstructure Physics, Weinberg 2, Halle (Saale), D-06120, Germany

[3]Department of Physics, University of Warwick, Coventry CV 4 7AL, United Kingdom

[4]The Pennsylvania State University, N-227 Millennium Science Complex, University Park, PA 16802, USA

[5]Universidad Complutense de Madrid, Madrid Spain

KEYWORDS: ferroelectric perovskite, $BiFeO_3$, atomic layer deposition, thin film

ABSTRACT: In this work, ferroelectricity is identified in nanocrystalline $BiFeO_3$ (BFO) thin films prepared by low temperature atomic layer deposition. A combination of X-ray diffraction, reflection high energy electron diffraction and scanning transmission electron microscopy analysis indicate that the as-deposited films (250ºC) consists of BFO nanocrystals embedded in an amorphous matrix. Post annealing at 650ºC for 60 min converts the sample to an epitaxial film on a $SrTiO_3$ substrate. Piezoelectric force microscopy demonstrates the existence of ferroelectricity in both as-deposited and post-annealed films. The ferroelectric behavior in the as-deposited stage is attributed to the presence of nanocrystals. Finally, a band gap of 2.71 eV was measured by spectroscopic ellipsometry. This study opens broad possibilities towards ferroelectric oxides on 3D substrates but also for the development of new ferroelectric perovskites prepared at low temperature.

Preparation of functional oxide thin films at very low temperatures, over large areas and compatible with low-cost and flexible substrates offers great industrial potential. Ferroelectric perovskite oxides[1] have received much attention for use in memory storage[2,3] micro-/nano-mechanical devices[4,5] and also for photovoltaics applications.[6-8] The degree of crystal perfection required for these perovskites varies according to specific application. However, in general, high temperature thermal treatments and textured growth are required for improved functional properties. This adds complexity in the materials processing in device integration. [2,9-17] One approach is to achieve locally high temperatures using laser annealing.[18-20] Alternatively, efforts have been made to develop new low-temperature synthesis routes for ferroelectric perovskite oxides; many of these are based on solution methodologies requiring processing temperatures of 300ºC- 400ºC.[21-23] The unique characteristics of conformality, atomic scale control and low temperature deposition that ALD technique offers can have direct technological applications: well controlled interfaces, smaller and more demanding structures (3D substrates), increased density of devices, including those that require flexible and transparent substrates, that have been hindered by the high temperature thermal treatment constraints.[17,24-27] This cost-effective chemical deposition technique is based on a self-limiting surface reaction mechanism that makes it very attractive for area-selective deposition. In principle, this could allow simultaneous patterning for the growing films, which offers some advantages for hard-to-pattern materials relative to traditional top-down patterning techniques. [28,29] ALD of ternary oxides such as perovskite oxides is still in its early stages.[30-32] Most as-deposited ALD films are amorphous or polycrystalline, although epitaxial oxides can also be obtained in the as-deposited stage (< 300ºC) using structurally compatible buffer layers and single crystal substrates.[33-36]

Among the ferroelectric perovskites, $BiFeO_3$ (BFO) is a stable, lead-free material that simultaneously presents ferroelectric and magnetic order at room temperature.[9,37-39] In the literature, resistive-switching and photovoltaic responses have also been reported.[7,40] Preparation of stoichiometric BFO thin films by ALD is challenging due to the limited number of potential bismuth precursor chemistries which are compatible with the iron precursor under the same ALD conditions. Also, the volatility of bismuth can lead to the formation of undesired second phases and/or film non-stoichiometry. [41-43]

In this work we show ferroelectricity of nanocrystalline BFO thin films prepared by ALD at 250ºC. The combination of X-ray diffraction, reflection high energy electron diffraction and scanning transmission electron microscopy analysis indicate that the as-deposited films consists of BFO nanocrystals embedded in an amorphous matrix : post annealing at 650ºC yields an epitaxial film. Piezoresponse force microscopy analysis demonstrates ferroelectricity in both as-deposited and post-annealed films. Finally, spectroscopic ellipsometry investigations on nanocrystalline BFO revealed a band gap energy of ~2.7 eV similar to that of bulk-BFO. These are encouraging results for ferroelectric perovskite oxides to break into many applications, including those that require flexible and transparent substrates, that have been hindered by the high temperature thermal treatment constraints.

Experimental

ALD of $BiFeO_3$ films. $BiFeO_3$ films were prepared in a Cambridge Nanotech Savannah flow-type reactor at 250ºC by alternate pulsing of bismuth tris(2,2,6,6-tetramethyl-3,5-heptanedionate) ($Bi(thd)_3$) and ferrocene ($Fe(Cp)_2$) combined with ozone (O_3). The precursor pulse ratio Bi/Fe was optimized to 2/1 using a pulse time of 2 s and a purge time of 20s with an average deposition rate of 0.02 nm/supercycle to obtain the required film stoichiometry (1Bi:1Fe). Atomic ratio quantification performed by XPS in the as-deposited and post-annealed sample is shown in Figure S3. The $Bi(thd)_3$ source was maintained at 175ºC and the $Fe(Cp)_2$ source at 90ºC. The number of supercycles was modified to achieve the desired film thickness. 5 x 5 mm^2 (100) strontium titanate (STO) substrates were cleaned by 5 minutes sonication in ethanol and dried with N_2. Each deposition run was performed simultaneously on STO(100) and thermally grown SiO_2/Si (100) substrates. Post-annealing treatment was carried out in a tube furnace in an oxygen atmosphere at 650ºC for 60 min.

$BiFeO_3$ structural characterization. Phase purity and film crystallinity were studied using Rigaku Rotaflex RU-200BV X-ray diffractometer with Cu-Kα λ=1.5418Å. Surface sensitive structural analysis was performed via Reflection High Energy Electron Diffraction (RHEED) in a kSA 400 RHEED system from k-Space inc., using an electron-gun acceleration voltage of 20 kV with 30 mA of beam current inside a UHV chamber. The incident angle of the incoming beam in respect to the surface plane was less than 3°, resulting in good surface sensitivity. Transmission electron microscopy (TEM) studies were performed by high angle annular dark field (HAADF) imaging in a probe aberration corrected JEOL ARM 200CF scanning transmission electron microscopy (STEM) with a cold field emission source operated at 200 kV, at Universidad Complutense de Madrid, Spain. The high angle annular dark field (HAADF) imaging mode yields Z-contrast images, in which the intensity of an atomic column is proportional to the square of the atomic number (Z). Specimens for STEM observations were prepared by conventional thinning, grinding, dimpling and Ar ion milling.

Ferroelectric characterization. Piezoelectric force microscopy measurements (PFM) were performed on BFO films prepared on Nb-doped strontium titanate (Nb:STO) substrates, with an Agilent 5500LS instrument equipped with a Signal Access Box and humidity conditions were kept below 5%. A DD-Sicona conducting tip (silicon, coated with boron-doped diamond) with a spring constant of 0.2 N/m was placed in direct contact with the BFO films. The AC frequency was set to ≈ 80 kHz, and its amplitude to 0.5V. PFM voltage hysteresis loops were performed after a dwell time of 3 ms for each voltage step. The cantilever deformation has been calibrated using a force-distance curve. The quantification of the displacement is detailed in the supporting information (Figure S5).

Chemical composition: XPS measurements were performed at room temperature with a SPECS PHOIBOS 150 hemispherical analyzer (SPECS GmbH, Berlin, Germany) in a base pressure of $1x10^{-10}$ mbar using monochromatic Al Kα radiation (1486.74 eV) as excitation source with a pass energy of 10 eV and step size of 0.05 eV for the high resolution spectra and 30 eV and 1 eV, respectively, for the survey spectra. To compensate charging effects, all spectra were calibrated with respect to the C1s peak at 284.9 eV. Spectra processing has been carried out after using a Shirley baseline for the background and Gaussian-Lorentzian curves to fit the different components.

Variable Angle Spectroscopic Ellipsometry : Variable angle spectroscopic ellipsometry (VASE) measurements were carried out using a SOPRALAB GES5E rotating polarizer ellipsometer that uses a Xe lamp as a light source and a CCD detector to record optical spectra from ca. 1.2 eV to 5.6 eV. For the analyzed system, the incorporation of a mixture roughness/air layer to the model does not modify the resulting optical parameters because of the BFO films are smooth, as observed from the topographic studies (see Figure 1 (d,e)). The optical parameters of the Nb:STO substrate were obtained from a separate set of measurements of the bare substrate performed at different incidence angles (50º, 60º and 70º).

Results

Preparation of ALD-BFO films with thicknesses ranging from 15 nm to 35 nm has been optimized on (100) STO and (100) Nb-STO single crystal substrates, as described in the Experimental section. As-deposited and post-annealed ALD BFO thin films were analyzed by X-ray diffraction (XRD) θ-2θ scans, see Figure 1(a). For the as-deposited films, no BFO reflections are identified, whereas for the post-annealed films (650ºC for 60 min), the characteristic BFO reflections are identified and indexed based on the pseudocubic indices.[44] The *c* lattice parameter obtained for the post annealed film is 3.93Å, very close to the bulk value of 3.96 Å, suggesting these films are largely relaxed. Note that there are two preferred orientations, (001) and (110). 2D-XRD θ-2θ shows that these two preferred orientations appear as bright spots, ruling out a polycrystalline growth (see supporting information Figure S1). Pole figure analysis reveal that the in-plane relationship of the (110) oriented BFO film with the STO substrate is [110]STO//[-110]BFO and [110]STO//[001]BFO, enabling a lattice matching of 1.1% and 7.2% respectively, see supporting information Figure S2. Importantly, no traces of the secondary phases typically reported during the formation of BFO films are observed (Bi_2O_3, Fe_2O_3, $Bi_2Fe_4O_9$).[41,45-48]

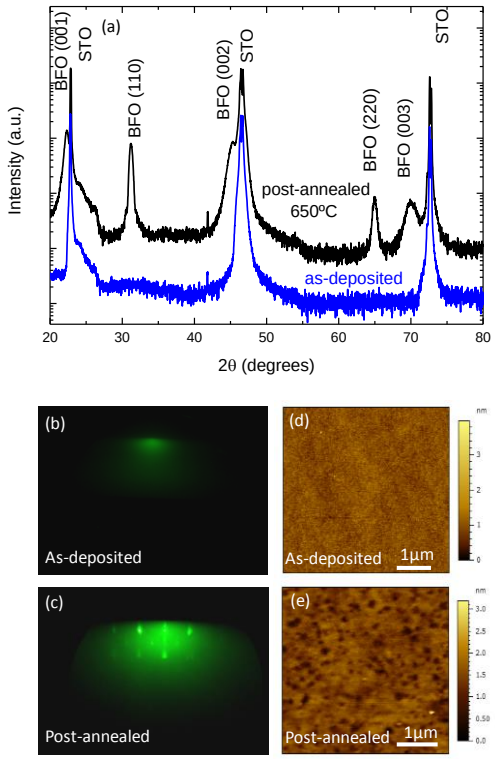

Figure 1. (a) X-ray diffraction θ-2θ scans of as-deposited and post-annealed films. (b) RHEED diffraction patterns for as-deposited and (c) post-annealed BFO films on (100) STO substrates. (d) 5 µm x 5 µm topographic image of as-deposited BFO film, and (e) annealed sample.

Ex-situ reflection high energy electron diffraction (RHEED) was carried out in as-deposited and post-annealed films. The resulting images are shown in Figures 1 b and 1c, respectively. It can be seen that the (0,0) constructive interference spot (the highest intensity mirror reflection spot) is only visible in the annealed case, although the measuring geometry of the two samples is exactly the same. This suggests that the surface in Figure 1(b) is amorphous and thus only allows diffuse reflection/scattering. The annealed film on the other hand (Fig 1c), shows clear cubic RHEED pattern, which unambiguously demonstrates the crystallinity of the film in the topmost area. The topographic images of as-deposited and annealed films, obtained by atomic force microscopy see Figure 1 (d,e), respectively, reveal an homogeneous and smooth surface with RMS of 0.3 nm for as-deposited and 1.1 nm for post annealed films.

X-ray photoelectron spectroscopy (XPS) analysis confirmed a cation ratio Fe:Bi of 1:1 in the as-deposit and post-annelaed stage (see Figure S3-S4). High resolution scans of the Bi(4f) and Fe(2p) regions are shown in Figure 2(a) and (b), respectively. The Bi(4f) spectrum shows a $Bi4f_{7/2}$ line centered at 158.9 eV, characteristic of the Bi-O bond[49]. From the Fe(2p) spectrum, binding energies for Fe $2p_{3/2}$ (710.7 eV), $Fe2p_{1/2}$ (724.2 eV) and the satellite peak (718.5 eV) were extracted, which corresponds well with reference values for Fe_2O_3.[49,50] Therefore, the XPS data indicate that Fe ions in ALD-BFO films are in the 3+ valence

state[51] although other authors also reported the coexistence of Fe^{2+} and Fe^{3+} in BFO thin films prepared by different thin film deposition techniques.[52,53]

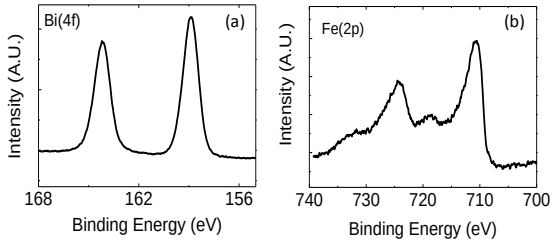

Figure 2. High resolution XPS spectra of as-deposited ALD-BFO films on Nb-$SrTiO_3$ substrates (a) Bi(4f) and (b)Fe(2p) regions.

Figure 3a,b exhibit two cross-sectional high resolution Z-contrast images of as-grown and annealed BFO layers grown onto STO, respectively. The as-grown layer (250ºC) consists mainly of a 35 nm thick amorphous matrix with homogeneously distributed polycrystalline BFO nanocrystals. The Figure 3a inset shows one of these nanoparticles with its corresponding FFT, which nucleated (110)-oriented on the surface substrate. Previous ALD studies on functional oxides performed in our group demonstrated that the low kinetics in ALD deposition can promote the formation of crystalline films at temperatures as low as 300ºC.[33,34] The surface of the as-grown layer is amorphous, which is in agreement with the RHEED results. In contrast, an annealing converts it into a fully crystalline layer. Figure 3b shows a region of (001)-oriented BFO layer with a sharp interface on the STO substrate. Yet, the scanning transmission electron microscopy (STEM) studies also show the presence of (110)-oriented grains in the post-annealed film (not shown), which is consistent with the X-ray analyses. Fully (110) BFO thin films can be epitaxially grown on lattice matched substrates such as (110) STO and (110) $DyScO_3$ single crystal substrates.[54,55]

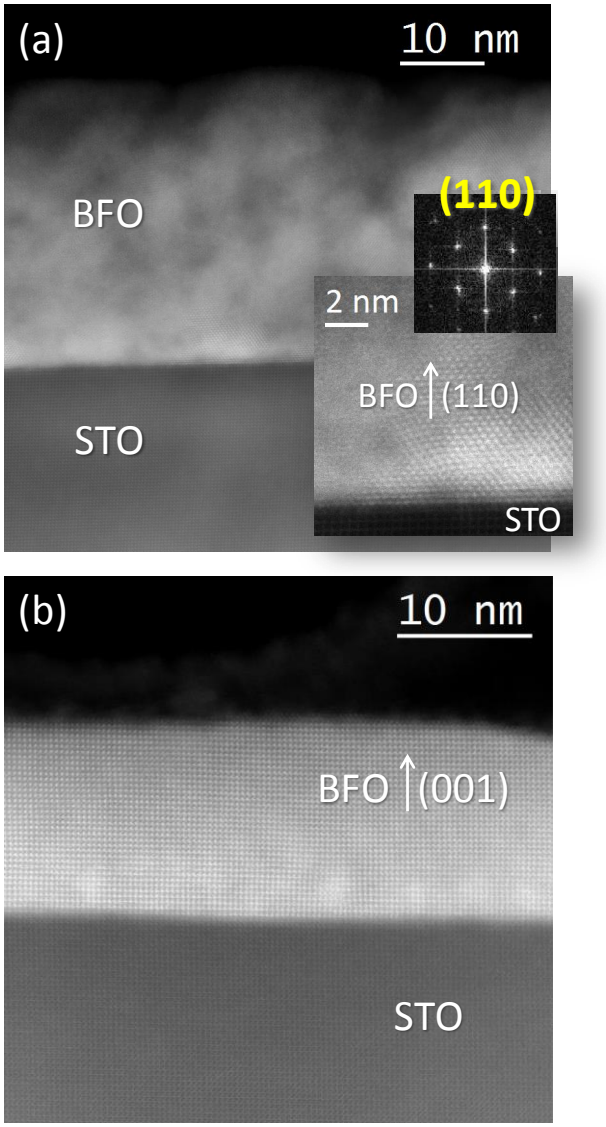

Figure 3. High resolution Z-contrast images of as-grown and annealed BFO layers grown on STO viewed along the <100> zone axis, (a) and (b), respectively. The inset in (a) shows the interface in detail, where a (110)-oriented BFO nanoparticle has nucleated. Its corresponding FFT shows the (110) reflection.

Piezoelectric force microscopy (PFM)[56] performed in a low-humidity atmosphere (<5%) was used to evaluate the ferroelectric nature of the BFO films on Nb:STO(100). The PFM-amplitude loop, Figure 4a, shows clear hysteretic behavior for as-deposited (blue) and post-annealed (black) samples, a signature of ferroelectric order. The ferroelectric nature of the samples is further supported by the 180º phase contrast of the PFM-phase loop shown in Figure 4b. The PFM displacement acquired at different AC voltages was used to extract the piezoelectric coefficient for both the as-deposited and annealed films, resulting in a d_{zz} = 4 pm/V and 17 pm/V, respectively (see Figure S3). These values are consistent with other reports for the piezoelectric coefficient of BFO thin films. [57] Figure 4c shows the PFM-phase image of the as-deposited sample after poling it with +8 and -8 V (P_{down}, pointing to the substrate, and P_{up} pointing to the film surface, respectively). The observed phase contrast reveals that: i) the polarization in the as-deposited sample is preferentially P_{up}, and ii) the ferroelectric polarization is retained over the time scale of the measurement (<30 min). A similar analysis performed on the annealed BFO layer is shown in Figure 4d and it shows a sharp phase contrast, revealing better retention properties compared to the as-deposited one.

Topography recorded simultaneously during the PFM imaging of the figure 4c-d demonstrates no surface degradation. This suggests that electrochemical process at the tip-surface junction during the electric writing did not dominate the results.[58,59] The presence of nanosized BFO crystals (~6 nm diameter) in the amorphous matrix of the as-deposited sample (250ºC) observed in the TEM analysis (Figure 3) could explain the ferroelectric response identified by PFM. Theoretical calculations suggested that the minimal critical thickness in which ferroelectricity can be sustained is down to 2 nm.[60,61]

Also, ferroelectric nanocrystals,[62] nanoislands,[63] self-assembled nanostructures[64] and nanorods[65] of ~ 3-5 nm have already been achieved for comparable crystalline size as the as-deposited ALD films. Therefore, it is likely that the nanosized ferroelectric crystals contribute to the ferroelectric nature of the BFO film. The amorphous matrix acts as a simple serial capacitance, lowering the retention of the ferroelectric polarization,[66] as revealed by the PFM analysis. These observations could explain what was previously identified as quasi-amorphous ferroelectrics[67-69] but strongly differs from an amorphous heteropolar electret.[2] On the other hand, the full crystallization of the film after appropriate annealing allows recovery of bulk-like properties (with better retention) of the epitaxial BFO film. Therefore, these results hold great potential to speed up ferroelectric oxide integration in more spatially demanding structures such as 3D semiconductor substrates for FeRAM, photovoltaic cells and nonvolatile reconfigurable logic.[17]

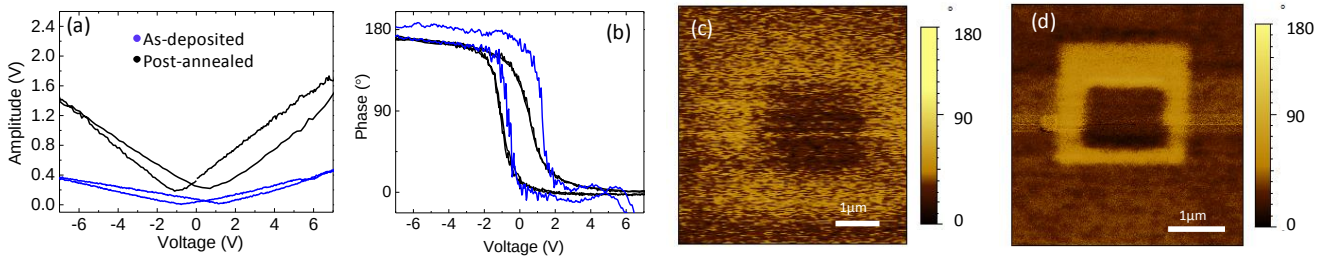

Figure 4. PFM analysis of as-deposited and post-annealed ALD BFO films on (100) Nb:STO substrates. (a) Piezo-amplitude and (b) Piezo-phase hysteresis loops of as-deposited and post-annealed samples. (c) Out-of-plane PFM phase image of as-deposited BFO on Nb:STO after switching a 4 µm x 4 µm area with V=-8V and switching back an inner square of 2 µm x 2 µm with DC bias of V=+8V. (d) out-of-plane PFM phase image of post-annealed film after switching a 2 µm x 2 µm area with DC bias of V=-8V and switching back an inner square of 1 µm x 1 µm with DC bias of V=+8V.

A crucial task towards achieving photoelectric applications is to establish the basic optical properties of the ALD BFO. The optical properties of as-deposited BFO thin films on Nb:STO have been evaluated by spectroscopic ellipsometry using a three-phase model consisting of air/BFO/Nb:STO, the experimental data were fitted according to the Tauc-Lorentz model.[70] Figure 5a displays the refractive index and extinction coefficient of as-deposited ALD-BFO films. The band gap was obtained from the extrapolation of αE^2 to zero leading a value of 2.71 ±0.04 eV, see figure 5b. The refractive index and extinction coefficient as well as the band gap are in good-agreement with the previously published data of BFO thin films.[71-73] This indicates that the optical properties of the low temperature as deposited ALD BFO are already in the interesting range. Further manipulation of the band gap to lower values by chemical doping (easy task by ALD), should open interesting avenues for photovoltaic applications of these oxide perovskites.[6,74]

Conclusions

Ferroelectric nanocrystalline BFO thin films were obtained in the as-deposited stage at 250ºC on STO(100) single crystals using atomic layer deposition. After a post-annealing treatment, the nanocrystalline film transforms to a relaxed epitaxial BFO film with improved ferroelectric properties. These findings offer a plethora of new opportunities from different stand-points. The use of ALD assures low-cost, large-area and uniform depositions with huge versatility to form ferroelectric perovskite oxides on 3D substrates including semiconductors, with different sizes and shapes. Also it will open a new arena for materials design favoring the preparation of a wide variety of ferroelectric perovskite compositions and to be extended to other functional complex oxide materials allowing future studies on their physical properties.

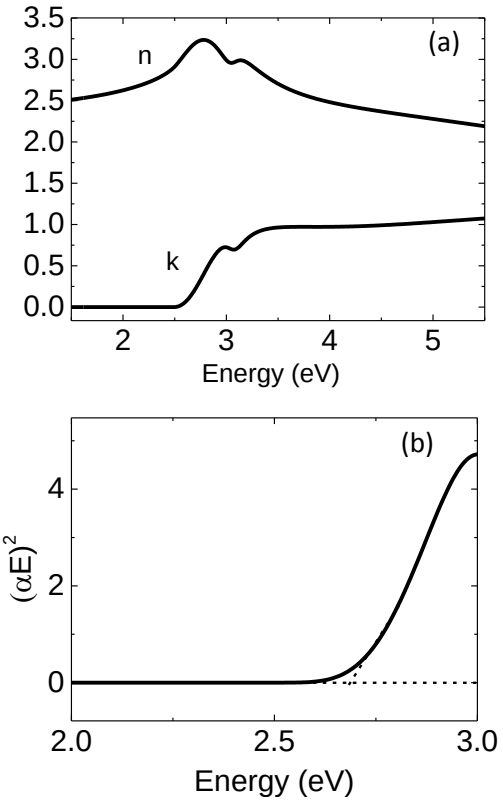

Figure 5.(a) Refractive index (n) and extinction coefficient (k) of as-deposited ALD-BFO thin films on Nb:STO obtained from fitting the measured ellipsometric data using a Tauc-Lorentz Model. (b) Plot of the αE^2 versus photon energy for the ALD-BFO films.

ASSOCIATED CONTENT

Supporting Information. 2D XRD characterization, XPS quantification and the deflection vs. V dependence of BFO films are given in detail. This material is available free of charge via the Internet at http:// pubs.acs.org.

AUTHOR INFORMATION

Corresponding Author

mcoll@icmab.es

Author Contributions

The manuscript was written through contributions of all authors. All authors have given approval to the final version of the manuscript.

Funding Sources

This research was supported by MAT2011-28874-C02-01, MAT2014-511778-C2-1-R and Consolider. M.C. and J.G acknowledges RyC contracts, 2013-12448 and 2012-11709, respectively. I.F. acknowledges the Beatriu de Pinós postdoctoral scholarship (2011 BP-A 00220) from AGAUR-Generalitat de Catalunya.Financial support from the ERC Starting investigator grant STEMOX 239739 and Consolider IMAGINE is acknowledged (M.V.).

ACKNOWLEDGMENT

We thank Mr. A. Gomez for the PFM measurements. We acknowledge the Scientific Services at ICMAB and G. Sauthier from ICN2 core support facilities for XPS analysis. Electron microscopy observations carried out at the ICTS-CNME at UCM. Authors acknowledge the ICTS-CNME for offering access to their instruments and expertise.

REFERENCES

(1) Heber, J. Materials science: Enter the oxides. *Nature* **2009**, *459*, 28-30.

(2) Lines, M. E.; Glass, A. M. *Principles and Applications of Ferroelectrics and Related Materials*; Clarendon Press: Oxford, 2001.

(3) Park, B. H.; Kang, B. S.; Bu, S. D.; Noh, T. W.; Lee, J.; Jo, W. Lanthanum-substituted bismuth titanate for use in non-volatile memories. *Nature* **1999**, *401*, 682-684.

(4) Eom, C. B.; Trolier-McKinstry, S. Thin-film piezoelectric MEMS. *MRS Bulletin* **2012**, *37*, 1007-1021.

(5) Mathews, S.; Ramesh, R.; Venkatesan, T.; Benedetto, J. Ferroelectric field effect transistor based on epitaxial perovskite heterostructures. *Science* **1997**, *276*, 238-240.

(6) Grinberg, I.; West, D. V.; Torres, M.; Gou, G. Y.; Stein, D. M.; Wu, L. Y.; Chen, G. N.; Gallo, E. M.; Akbashev, A. R.; Davies, P. K.; Spanier, J. E.; Rappe, A. M. Perovskite oxides for visible-light-absorbing ferroelectric and photovoltaic materials. *Nature* **2013**, *503*, 509-512.

(7) Choi, T.; Lee, S.; Choi, Y. J.; Kiryukhin, V.; Cheong, S. W. Switchable Ferroelectric Diode and Photovoltaic Effect in $BiFeO_3$. *Science* **2009**, *324*, 63-66.

(8) Kim, D. M.; Gallagher, J. G.; Rabson, T. A.; Tittel, F. K. Intensity Enhanced Bulk Photo-Voltaic Effects in $LiNbO_3$-Fe. *Appl Phys* **1978**, *17*, 413-416.

(9) Wang, J.; Neaton, J. B.; Zheng, H.; Nagarajan, V.; Ogale, S. B.; Liu, B.; Viehland, D.; Vaithyanathan, V.; Schlom, D. G.; Waghmare, U. V.; Spaldin, N. A.; Rabe, K. M.; Wuttig, M.; Ramesh, R. Epitaxial $BiFeO_3$ multiferroic thin film heterostructures. *Science* **2003**, *299*, 1719-1722.

(10) Catalan, G.; Noheda, B.; McAneney, J.; Sinnamon, L. J.; Gregg, J. M. Strain gradients in epitaxial ferroelectrics. *Physical Review B* **2005**, *72*, 020102.

(11) Tybell, T.; Ahn, C. H.; Triscone, J. M. Ferroelectricity in thin perovskite films. *Appl Phys Lett* **1999**, *75*, 856-858.

(12) Park, S. E.; Shrout, T. R. Ultrahigh strain and piezoelectric behavior in relaxor based ferroelectric single crystals. *Journal of Applied Physics* **1997**, *82*, 1804-1811.

(13) Dawber, M.; Rabe, K. M.; Scott, J. F. Physics of thin-film ferroelectric oxides. *Rev Mod Phys* **2005**, *77*, 1083-1130.

(14) Shaw, T. M.; Trolier-McKinstry, S.; McIntyre, P. C. The properties of ferroelectric films at small dimensions. *Annu Rev Mater Sci* **2000**, *30*, 263-298.

(15) Setter, N.; Damjanovic, D.; Eng, L.; Fox, G.; Gevorgian, S.; Hong, S.; Kingon, A.; Kohlstedt, H.; Park, N. Y.; Stephenson, G. B.; Stolitchnov, I.; Taganstev, A. K.; Taylor, D. V.; Yamada, T.; Streiffer, S. Ferroelectric thin films: Review of materials, properties, and applications. *Journal of Applied Physics* **2006**, *100*, 051606.

(16) Farokhipoor, S.; Magen, C.; Venkatesan, S.; Iniguez, J.; Daumont, C. J. M.; Rubi, D.; Snoeck, E.; Mostovoy, M.; de Graaf, C.; Muller, A.; Doblinger, M.; Scheu, C.; Noheda, B. Artificial chemical and magnetic structure at the domain walls of an epitaxial oxide. *Nature* **2014**, *515*, 379-383.

(17) Ponath, P.; Fredrickson, K.; Posadas, A. B.; Ren, Y.; Wu, X. Y.; Vasudevan, R. K.; Okatan, M. B.; Jesse, S.; Aoki, T.; McCartney, M. R.; Smith, D. J.; Kalinin, S. V.; Lai, K.; Demkov, A. A. Carrier density modulation in a germanium heterostructure by ferroelectric switching. *Nature Communications* **2015**, *6*, 6067.

(18) Nakajima, T.; Shinoda, K.; Tsuchiya, T. UV-assisted nucleation and growth of oxide films from chemical solutions. *Chemical Society Reviews* **2014**, *43*, 2027-2041.

(19) Paetzel, R.; Turk, B.; Brune, J.; Govorkov, S.; Simon, F. Lasers solutions for wafer and thin-film annealing. *physica status solidi (c)* **2008**, *5*, 3215-3220.

(20) Bharadwaja, S. S. N.; Kulik, J.; Akarapu, R.; Beratan, H.; Trolier McKinstry, S. Ultrafast crystallization kinetics in $(Pb,La)(Zr_{0.30}Ti_{0.70})O_3$ thin films by pulsed excimer laser annealing. *IEEE Transactions on Ultrasonics, Ferroelectrics and Frequency Control* **2010**, *57*, 2182-2191.

(21) Bretos, I.; Jimenez, R.; Wu, A. Y.; Kingon, A. I.; Vilarinho, P. M.; Calzada, M. L. Activated Solutions Enabling Low-Temperature Processing of Functional Ferroelectric Oxides for Flexible Electronics. *Adv. Mater.* **2014**, *26*, 1405-1409.

(22) Malic, B.; Mandeljc, M.; Malič, B.; Kosec, M. PZT Thin Films with Decreasing Thickness Crystallized at 400°C. *Integr Ferroelectr* **2003**, *52*, 205-213.

(23) Calzada, M. L.; Bretos, I.; Jiménez, R.; Guillon, H.; Pardo, L. Low-Temperature Processing of Ferroelectric Thin Films Compatible with Silicon Integrated Circuit Technology. *Adv. Mater.* **2004**, *16*, 1620-1624.

(24) Pinna, N.; Knez, M. *Atomic Layer Deposition of Nanostructured Materials*; Wiley-VCH Germany, 2012.

(25) Parsons, G. N.; George, S. M.; Knez, M. Progress and future directions for atomic layer deposition and ALD-based chemistry. *MRS Bulletin* **2011**, *36*, 865-871.

(26) Lubitz, M.; Medina, P. A.; Antic, A.; Rosin, J. T.; Fahlman, B. D. Cost-Effective Systems for Atomic Layer Deposition. *J Chem Educ* **2014**, *91*, 1022-1027.

(27) International Technology Roadmap for Semiconductors, Emerging Research Materials Summary. **2013**.

(28) Mackus, A. J. M.; Bol, A. A.; Kessels, W. M. M. The use of atomic layer deposition in advanced nanopatterning. *Nanoscale* **2014**, *6*, 10941-10960.

(29) Bae, C.; Shin, H.; Nielsch, K. Surface modification and fabrication of 3D nanostructures by atomic layer deposition. *MRS Bulletin* **2011**, *36*, 887-897.

(30) Murray, C.; Elliott, S. D. Density Functional Theory Predictions of the Composition of Atomic Layer Deposition-Grown Ternary Oxides. *ACS Applied Materials & Interfaces* **2013**, *5*, 3704-3715.

(31) Leskelä, M.; Ritala, M.; Nilsen, O. Novel materials by atomic layer deposition and molecular layer deposition. *MRS Bulletin* **2011**, *36*, 877-884.

(32) Wiemer, C.; Lamagna, L.; Fanciulli, M. Atomic layer deposition of rare-earth-based binary and ternary oxides for microelectronic applications. *Semicond. Sci. Technol.* **2012**, *27*, 074013.

(33) Coll, M.; Montero Moreno, J. M.; Gazquez, J.; Nielsch, K.; Obradors, X.; Puig, T. Low Temperature Stabilization of Nanoscale Epitaxial Spinel Ferrite Thin Films by Atomic Layer Deposition. *Advanced Functional Materials* **2014**, *24*, 5368-5374.

(34) Coll, M.; Gazquez, J.; Palau, A.; Varela, M.; Obradors, X.; Puig, T. Low Temperature epitaxial ultrathin film oxides and nanostructures by atomic layer deposition *Chemistry of Materials* **2012**, *24*, 3732-3737.

(35) Ngo, T.; Posadas, A.; McDaniel, M.; Hu, C.; Bruley, J.; Yu, E.; Demkov, A.; Ekerdt, J. Epitaxial c-axis oriented $BaTiO_3$ thin films on $SrTiO_3$-buffered Si(001) by atomic layer deposition. *Appl Phys Lett* **2014**, *104*, 082910.

(36) Coll, M.; Palau, A.; Gonzalez-Rosillo, J.; Gazquez, J.; Obradors, X.; Puig, T. Integration of ALD CeO_2 thin films with functional complex oxides and 3D patterns *Thin Solid Films* **2014**, *553*, 7-12.

(37) Spaldin, N. A.; Cheong, S. W.; Ramesh, R. Multiferroics: Past, present, and future. *Phys Today* **2010**, *63*, 38-43.

(38) Catalan, G.; Scott, J. F. Physics and Applications of Bismuth Ferrite. *Adv. Mater.* **2009**, *21*, 2463-2485.

(39) Sando, D.; Barthelemy, A.; Bibes, M. $BiFeO_3$ epitaxial thin films and devices: past, present and future. *J Phys-Condens Mat* **2014**, *26*, 473201

(40) Yang, C. H.; Seidel, J.; Kim, S. Y.; Rossen, P. B.; Yu, P.; Gajek, M.; Chu, Y. H.; Martin, L. W.; Holcomb, M. B.; He, Q.; Maksymovych, P.; Balke, N.; Kalinin, S. V.; Baddorf, A. P.; Basu, S. R.; Scullin, M. L.; Ramesh, R. Electric modulation of conduction in multiferroic Ca-doped $BiFeO_3$ films. *Nat Mater* **2009**, *8*, 485-493.

(41) Akbashev, A. R.; Chen, G.; Spanier, J. E. A Facile Route for Producing Single-Crystalline Epitaxial Perovskite Oxide Thin Films. *Nano Letters* **2014**, *14*, 44-49.

(42) Zhang, F.; Sun, G. S.; Zhao, W. S.; Wang, L.; Zeng, L.; Liu, S. B.; Liu, B.; Dong, L.; Liu, X. F.; Yan, G. G.; Tian, L. X.; Zeng, Y. P. Atomic Layer Deposition of $BiFeO_3$ Thin Films Using beta-Diketonates and H_2O. *J Phys Chem C* **2013**, *117*, 24579-24585.

(43) Liu, Y.-T.; Ku, C.-S.; Chiu, S.-J.; Lee, H.-Y.; Chen, S.-Y. Ultrathin Oriented $BiFeO_3$ Films from Deposition of Atomic Layers with Greatly Improved Leakage and Ferroelectric Properties. *ACS Applied Materials & Interfaces* **2014**, *6*, 443-449.

(44) Achenbac.Gd; James, W. J.; Gerson, R. Preparation of Single-Phase Polycrystalline $BiFeo_3$. *Journal of the American Ceramic Society* **1967**, *50*, 437.

(45) Iakovlev, S.; Solterbeck, C.-H.; Kuhnke, M.; Es-Souni, M. Multiferroic $BiFeO_3$ thin films processed via chemical solution deposition: Structural and electrical characterization. *Journal of Applied Physics* **2005**, *97*, 094901

(46) Thery, J.; Dubourdieu, C.; Baron, T.; Ternon, C.; Roussel, H.; Pierre, F. MOCVD of $BiFeO_3$ thin films on $SrTiO_3$. *Chem. Vapor Depos.* **2007**, *13*, 232-238.

(47) Fujino, S.; Murakami, M.; Lim, S. H.; Wuttig, M.; Salamanca-Riba, L. G.; Takeuchi, I. Ferroelectric properties of multiphase Bi-Fe-O thin films. *Solid State Ionics* **2007**, *178*, 1257-1261.

(48) You, L.; Chua, N. T.; Yao, K.; Chen, L.; Wang, J. L. Influence of oxygen pressure on the ferroelectric properties of epitaxial $BiFeO_3$ thin films by pulsed laser deposition. *Physical Review B* **2009**, *80*, 024105.

(49) Chastain, J.; Moulder, J. F. *Handbook of X-ray Photoelectron Spectroscopy: A Reference Book of Standard Spectra for Identification and Interpretation of XPS Data*; Physical Electronics, 1995.

(50) Fujimori, A.; Saeki, M.; Kimizuka, N.; Taniguchi, M.; Suga, S. Photoemission Satellites and Electronic-Structure of Fe_2O_3. *Physical Review B* **1986**, *34*, 7318-7333.

(51) Kozakov, A. T.; Kochur, A. G.; Googlev, K. A.; Nikolsky, A. V.; Raevski, I. P.; Smotrakov, V. G.; Yeremkin, V. V. X-ray photoelectron study of the valence state of iron in iron-containing single-crystal ($BiFeO_3$, $PbFe_{1/2}Nb_{1/2}O_3$), and ceramic ($BaFe_{1/2}Nb_{1/2}O_3$) multiferroics. *Journal of Electron Spectroscopy and Related Phenomena* **2011**, *184*, 16-23.

(52) Eerenstein, W.; Morrison, F. D.; Dho, J.; Blamire, M. G.; Scott, J. F.; Mathur, N. D. Comment on "Epitaxial $BiFeO_3$ multiferroic thin film heterostructures". *Science* **2005**, *307*, 1203-1203.

(53) Wang, J.; Scholl, A.; Zheng, H.; Ogale, S. B.; Viehland, D.; Schlom, D. G.; Spaldin, N. A.; Rabe, K. M.; Wuttig, M.; Mohaddes, L.; Neaton, J.; Waghmare, U.; Zhao, T.; Ramesh, R. Response to comment on "Epitaxial $BiFeO_3$ multiferroic thin film heterostructures". *Science* **2005**, *307*, 1203b.

(54) Chu, Y. H.; Cruz, M. P.; Yang, C. H.; Martin, L. W.; Yang, P. L.; Zhang, J. X.; Lee, K.; Yu, P.; Chen, L. Q.; Ramesh, R. Domain Control in Multiferroic $BiFeO_3$ through Substrate Vicinality. *Adv. Mater.* **2007**, *19*, 2662-2666.

(55) Zavaliche, F.; Yang, S. Y.; Zhao, T.; Chu, Y. H.; Cruz, M. P.; Eom, C. B.; Ramesh, R. Multiferroic $BiFeO_3$ films: domain structure and polarization dynamics. *Phase Transit* **2006**, *79*, 991-1017.

(56) Kalinin, S. V.; Morozovska, A. N.; Chen, L. Q.; Rodriguez, B. J. Local polarization dynamics in ferroelectric materials. *Rep Prog Phys* **2010**, *73*, 056502.

(57)*www.asylumresearch.com/Applications/PFMAppNote/PFMAppNote.shtml*.

(58) Kalinin, S. V.; Jesse, S.; Tselev, A.; Baddorf, A. P.; Balke, N. The role of electrochemical phenomena in scanning probe microscopy of ferroelectric thin films. *ACS Nano* **2011**, *5*, 5683-5691.

(59) Arruda, T. M.; Kumar, A.; Kalinin, S. V.; Jesse, S. Mapping irreversible electrochemical processes on the nanoscale: Ionic phenomena in Li ion conductive glass ceramics. *Nano Letters* **2011**, *11*, 4161-4167.

(60) Junquera, J.; Ghosez, P. Critical thickness for ferroelectricity in perovskite ultrathin films. *Nature* **2003**, *422*, 506-509.

(61) Ahn, C. H.; Rabe, K. M.; Triscone, J. M. Ferroelectricity at the nanoscale: Local polarization in oxide thin films and heterostructures. *Science* **2004**, *303*, 488-491.

(62) Polking, M. J.; Han, M. G.; Yourdkhani, A.; Petkov, V.; Kisielowski, C. F.; Volkov, V. V.; Zhu, Y. M.; Caruntu, G.; Alivisatos, A. P.; Ramesh, R. Ferroelectric order in individual nanometre-scale crystals. *Nat Mater* **2012**, *11*, 700-709.

(63) Tiedke, S.; Schmitz, T.; Prume, K.; Roelofs, A.; Schneller, T.; Kall, U.; Waser, R.; Ganpule, C. S.; Nagarajan, V.; Stanishevsky, A.; Ramesh, R. Direct hysteresis measurements of single nanosized ferroelectric capacitors contacted with an atomic force microscope. *Appl Phys Lett* **2001**, *79*, 3678-3680.

(64) Szafraniak, I.; Harnagea, C.; Scholz, R.; Bhattacharyya, S.; Hesse, D.; Alexe, M. Ferroelectric epitaxial nanocrystals obtained by a self-patterning method. *Appl Phys Lett* **2003**, *83*, 2211-2213.

(65) Yun, W. S.; Urban, J. J.; Gu, Q.; Park, H. Ferroelectric properties of individual barium titanate nanowires investigated by scanned probe Microscopy. *Nano Letters* **2002**, *2*, 447-450.

(66) Ma, T. P.; Han, J. P. Why is nonvolatile ferroelectric memory field-effect transistor still elusive? *Ieee Electr Device L* **2002**, *23*, 386-388.

(67) Wachtel, E.; Lubomirsky, I. Quasi-amorphous inorganic thin films: Non-crystalline polar phases. *Adv. Mater.* **2010**, *22*, 2485-2493.

(68) Wang, J. L.; Pancotti, A.; Jegou, P.; Niu, G.; Gautier, B.; Jégou, P.; Mi, Y. Y.; Tortech, L.; Yin, S.; Vilquin, B.; Barrett, N. Ferroelectricity in a quasiamorphous ultrathin $BaTiO_3$ film. *Physical Review. B, Condensed Matter and Materials Physics* **2011**, *84*, 205426.

(69) Mackenzie, J. D.; Xu, Y. H. Ferroelectric materials by the sol-gel method. *J Sol-Gel Sci Techn* **1997**, *8*, 673-679.

(70) Jellison, G. E.; Modine, F. A. Parameterization of the optical functions of amorphous materials in the interband region. *Appl Phys Lett* **1996**, *69*, 371-373.

(71) Kumar, A.; Rai, R. C.; Podraza, N. J.; Denev, S.; Ramirez, M.; Chu, Y. H.; Martin, L. W.; Ihlefeld, J.; Heeg, T.; Schubert, J.; Schlom, D. G.; Orenstein, J.; Ramesh, R.; Collins, R. W.; Musfeldt, J. L.; Gopalan, V. Linear and nonlinear optical properties of BiFeO(3). *Appl Phys Lett* **2008**, *92*, 121915.

(72) Himcinschi, C.; Vrejoiu, I.; Friedrich, M.; Nikulina, E.; Ding, L.; Cobet, C.; Esser, N.; Alexe, M.; Rafaja, D.; Zahn, D. R. T. Substrate influence on the optical and structural properties of pulsed laser deposited BiFeO3 epitaxial films. *Journal of Applied Physics* **2010**, *107*, 123524.

(73) Bhatnagar, A.; Kim, Y. H.; Hesse, D.; Alexe, M. Sub-band level-assisted photoconduction in epitaxial $BiFeO_3$ films. *Appl Phys Lett* **2014**, *105*, 122905.

(74) Wang, F. G.; Grinberg, I.; Rappe, A. M. Band gap engineering strategy via polarization rotation in perovskite ferroelectrics. *Appl Phys Lett* **2014**, *104*, 152903.

SYNOPSIS TOC. Ferroelectric nanocrystalline BiFeO3 thin films with promising optical properties prepared by low temperature atomic layer deposition